SINERGI Vol. 30, No. 1, February 2026: 79-90
http://publikasi.mercubuana.ac.id/index.php/sinergi
http://doi.org/10.22441/sinergi.2026.1.008

An ultra-broadband microstrip antenna using a triple dumbbell-shaped defected ground structure

Puji Haryanto[1], Dian Widi Astuti[1,*], Mudrik Alaydrus[1], Ahmad Firdausi[1], Dian Rusdiyanto[1], Huda A Majid[2]
[1]Electrical Engineering Department, Faculty of Engineering, Universitas Mercu Buana, Indonesia
[2]Department of Electrical Engineering, Faculty of Engineering Technology, Universiti Tun Hussein Onn Malaysia, Malaysia

Abstract
Microstrip antennas are widely used in modern communication systems due to their compact size and low profile. However, they typically suffer from narrow bandwidth, limiting their performance in advanced wireless applications. This study addresses this limitation by employing a triple dumbbell-shaped defected ground structure (DGS). The antenna is designed to operate at 3.5 GHz using a Rogers RT5880 substrate, and its performance was analyzed through simulations in HFSS 15.0 software. Without the DGS, the antenna exhibits a fractional bandwidth (FBW) of only 1.71%, operating from 3.47 GHz to 3.53 GHz. Incorporating the triple dumbbell-shaped DGS in the ground layer increases the FBW significantly to 53.6%, extending the operating frequency range from 2.39 GHz to 4.14 GHz. This improvement was achieved through the careful optimization of DGS parameters. The simulated gain at 3.5 GHz is 5.13 dBi. The proposed design demonstrates superior performance compared to conventional techniques such as split-ring resonators (SRR) and Butler matrix (BM) configurations. Simulation and measurement results show excellent agreement, validating the design. The achieved ultra-wideband performance benefits 5G and next-generation systems, offering greater frequency tolerance, diverse signal support, increased capacity, and reliable operation, making the antenna a promising candidate for future wireless applications.

Keywords:
5G Ultra-broadband;
Bandwidth enhancement;
Defected Ground Structure;
Microstrip Antenna;

Article History:
Received: March 24, 2025
Revised: September 12, 2025
Accepted: October 2, 2025
Published: January 7, 2026

Corresponding Author:
Dian Widi Astuti
Department of Electrical Engineering, Faculty of Engineering, Universitas Mercu Buana, Indonesia
Email:
dian.widiastuti@mercubuana.ac.id

INTRODUCTION

The rapid development of 5G technology in Indonesia has driven the need for advanced wireless communication systems that support higher data rates, low latency, and reliable connectivity for a wide range of applications, including high-definition video streaming, industrial automation, autonomous vehicles, and the Internet of Things (IoT) [1]. These applications demand antennas with wide operational bandwidth, high efficiency, stable radiation patterns, and robust performance across multiple frequency bands. The design of compact, low-cost, and ultra-broadband antennas has therefore become a critical challenge in modern telecommunications.

Microstrip antennas are widely adopted in modern wireless systems due to their compact size, low profile, lightweight structure, and ease of integration with printed circuit boards (PCBs) [2]. Their planar geometry allows for simple fabrication and mass production, making them attractive for consumer electronics, IoT devices, and communication infrastructure. Despite these advantages, conventional microstrip antennas are typically limited by narrow impedance bandwidth and single-frequency operation, which restricts their use in wideband or multi-band systems [3][4].

To overcome these limitations, researchers have explored a variety of bandwidth enhancement techniques. Among them, Defected Ground Structures (DGS) have proven effective in improving impedance bandwidth, reducing mutual coupling, and enhancing radiation characteristics [5-18]. Other approaches include split-ring resonators (SRR) [19][20], Butler Matrix (BM) configurations [21][22], parasitic elements [23], and truncated microstrip patches [24]. Each technique provides unique benefits: SRR and BM methods can improve phase control and bandwidth, parasitic elements enhance isolation in MIMO systems, and truncated designs allow compactness and miniaturization. However, despite these improvements, most methods remain inadequate for ultra-broadband applications, with fractional bandwidths (FBW) typically below 50%.

Conventional DGS configurations, including rectangular, circular, or single dumbbell-shaped slots, generally achieve FBW between 20% and 40% [5-18]. Hybrid methods combining DGS with other techniques or advanced substrates, such as magneto-dielectric (MD) materials and multi-walled carbon nanotube (MWCNT) composites, have reported FBW improvements up to 30% or higher [19-22]. While these designs improve performance, they introduce fabrication complexity and require precise optimization of dimensions, materials, and geometries. Other methods, including BM and parasitic elements, provide selective advantages but are either limited in bandwidth improvement or involve complex design procedures [21, 22 23]. Truncated microstrip patch antennas with complementary split-ring resonators show bandwidth enhancement and size reduction, but still fall short of true ultra-broadband operation [24].

Several studies have demonstrated incremental improvements in FBW using advanced DGS designs. For example, references [7-10] report FBW improvements from 5.09% to 38% over frequency ranges from 2.4 GHz to 40.9 GHz. Hybrid and material-assisted methods have achieved FBW up to 48.67% [19][20]. Although these results are promising, they often require complex fabrication processes, intricate optimization, or additional components, making them less practical for cost-effective and reproducible antenna designs. These observations highlight the need for a simple yet efficient approach to achieve ultra-broadband performance.

To address these limitations, the present study proposes a triple dumbbell-shaped DGS, introducing three sequential dumbbell slots beneath the microstrip patch. This configuration increases the effective current path and coupling in the ground plane, which reduces the antenna's Q-factor and significantly broadens impedance bandwidth. By carefully optimizing the dimensions and positions of the dumbbell slots, the design enhances resonant mode interaction and minimizes reflection losses. This strategy differentiates the proposed antenna from conventional single or hybrid DGS designs and provides a systematic method to achieve ultra-broadband operation.

The proposed antenna demonstrates a simulated FBW of 53.6% and a measured FBW of 51.4%, exceeding the 50% threshold commonly used to classify ultra-broadband antennas. The design maintains structural simplicity, allowing easy fabrication with standard PCB techniques. Simulation and experimental results show excellent agreement, confirming the effectiveness of the triple dumbbell-shaped DGS in enhancing bandwidth while maintaining desirable radiation characteristics. The design outperforms conventional DGS, SRR, and BM-based antennas in both bandwidth and overall system simplicity.

The enhanced ultra-broadband performance of the proposed antenna enables support for diverse signal types, increases system capacity, and ensures reliable operation for 5G and next-generation wireless communication systems. Its compact size, high efficiency, and cost-effective fabrication make it suitable for practical applications such as IoT devices, WLAN, RFID, and other wireless infrastructure. By providing a simple yet highly effective solution, this work contributes to the advancement of broadband microstrip antenna design and offers a promising candidate for future wireless communication technologies.

METHOD

Based on previous research, a microstrip antenna operating at 3.5 GHz for 5G applications has been proposed, utilizing the DGS method to enhance performance. The triple dumbbell-shaped DGS is specifically employed to broaden the antenna's bandwidth, addressing limitations identified in earlier studies. This research encompasses the entire process of planning, fabrication, and measurement of the antenna to evaluate its performance and validate the effectiveness of the DGS approach.

During the antenna design phase, HFSS 15.0 software is utilized for simulations, comparing a conventional microstrip antenna without DGS to a microstrip antenna

incorporating DGS. Microstrip antennas are known for their simplicity but often suffer from narrow bandwidth, which this study aims to address. The research focuses on how a dumbbell-shaped DGS can effectively enhance the bandwidth of microstrip antennas operating at 3.5 GHz. The researchers' work builds on previous studies and seeks to improve results in broadening the bandwidth of microstrip antennas by implementing the dumbbell-shaped DGS.

The main contributions and novelty of this work are summarized as follows:

1. Ultra-broadband performance via triple dumbbell-shaped DGS:
   This study introduces a triple dumbbell-shaped defected ground structure (DGS) to significantly enhance the fractional bandwidth (FBW) of microstrip antennas. Compared to conventional designs with an FBW of 1.71%, the proposed design achieves an FBW of 53.6% at 3.5 GHz, specifically targeting 5G applications. This demonstrates that the novel triple dumbbell-shaped DGS effectively overcomes the narrow bandwidth limitation and achieves ultra-wideband operation, which has not been reported in prior DGS-based designs.
2. Systematic optimization of DGS parameters for superior performance:
   A comprehensive optimization of the DGS geometry—including length, width, and height of the dumbbell slots—was conducted to maximize bandwidth and minimize reflection (S11). The optimized design (length = 40 mm, width = 2 mm, height = 8 mm) achieves the lowest S11 of -33.68 dB and FBW of 53.6%, demonstrating the effectiveness of precise parameter tuning. This provides a practical guideline for designing high-performance microstrip antennas with DGS, emphasizing both novelty and applicability in modern wireless communication systems.

Material

The microstrip antenna designed in this research uses the Rogers RT5880 substrate, which has a thickness of 1.575 mm and a permittivity of 2.2, offering excellent characteristics for antenna performance. Conventional techniques for enhancing bandwidth, such as SRR, BM, and parasitic elements, are often employed in antenna design. However, these methods tend to offer only marginal improvements or require complex designs, which can limit their practical applicability.

Previous studies on microstrip antennas with DGS have often failed to fully exploit the potential of specific configurations, such as dumbbell-shaped structures, leaving room for further optimization, especially at 3.5 GHz for 5G applications. This research applies established electromagnetic theory to achieve significant performance improvements, which are rigorously validated through both simulation and measurement. The goal of this study is to design and validate a microstrip antenna with enhanced bandwidth at 3.5 GHz, making it suitable for modern 5G applications, particularly in Indonesia [10][25].

Conventional Antenna Design

In the initial stage, a conventional antenna design is developed to understand the basic characteristics of microstrip antennas without any additional modifications. This stage involves discussing the conventional antenna design process, focusing on its fundamental design principles and parameters. The performance results from this design are evaluated and used as a reference for subsequent stages of modification aimed at improving antenna performance.

Figure 1 illustrates the basic design of the microstrip antenna without any additional modifications. This initial design serves as a reference point for evaluating the antenna's performance before any changes are made. Figure 2 presents the frequency performance, as shown by the S_{11} graph, covering a frequency range of 3.47–3.53 GHz. The graph highlights a main resonant point near 3.5 GHz, where the S_{11} value is notably low, around -22 dB. This low S_{11} value indicates that most of the RF (Radio Frequency) power is successfully received by the antenna, with minimal reflection.

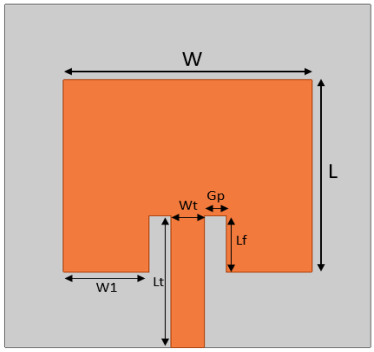

Figure 1. The conventional antenna design (without DGS structure) has dimensions: *W* = 34 mm, *L* = 28 mm, *W*1 = 11.75 mm, *Lf* = 8.2 mm, *Gp* = 3 mm, *Lt* = 19.2 mm, *Wt* = 4.5 mm

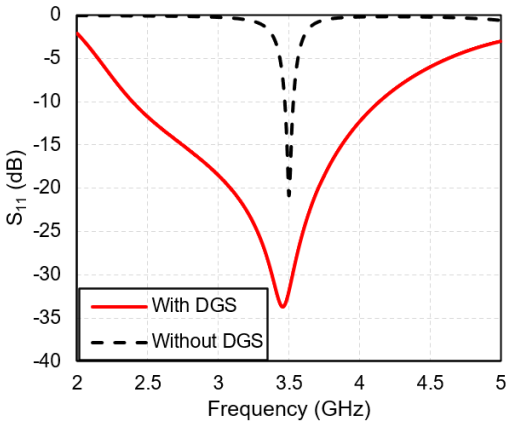

Figure 2. S_{11} simulation results of the conventional antenna with and without DGS structures

Microstrip Antenna Design with triple dumbbell-shaped DGS

In general, a defected ground structure (DGS) introduces a disturbance in the ground-plane current distribution, which can be modeled as an equivalent inductive–capacitive (LC) network. This perturbation modifies the input impedance of the antenna and is often used to improve matching and increase bandwidth. In the proposed design, triple dumbbell-shaped DGS-shaped slots are etched sequentially beneath the patch. The presence of multiple dumbbells produces a stronger perturbation of the surface current compared to conventional single or double triple dumbbell-shaped DGS. As a result, the impedance matching is significantly improved across a wider frequency range. This mechanism broadens the single resonant mode into an ultra-wideband response, while maintaining a low return loss (S11) at resonance. Therefore, the proposed triple dumbbell-shaped DGS provides a clear improvement over conventional DGS techniques, which typically achieve only 20–40% fractional bandwidth.

The simulated surface current distribution confirms this behavior. Compared to the antenna without DGS or with a single dumbbell slot, the proposed triple dumbbell configuration shows a stronger perturbation of the ground current and a more uniform distribution beneath the patch. This effect results in better impedance matching across the operating band, which is consistent with the measured S11 characteristics and the observed ultra-wideband performance.

Figure 3 shows the evolution of the antenna designs. The microstrip antenna is designed with a dumbbell-shaped DGS. The evolution of antenna design starts from Antenna 1, Antenna 2, and Antenna 3. Every antenna design varies with the number of dumbbells.

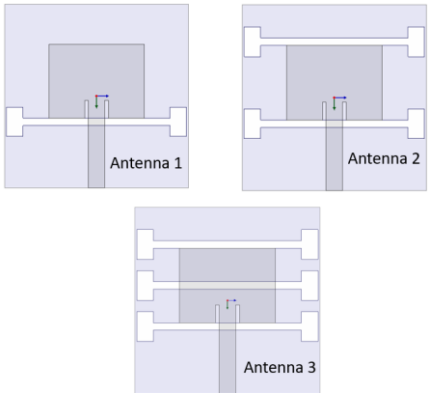

Figure 2. The microstrip antenna evolution design with several Triple dumbbell-shaped DGS

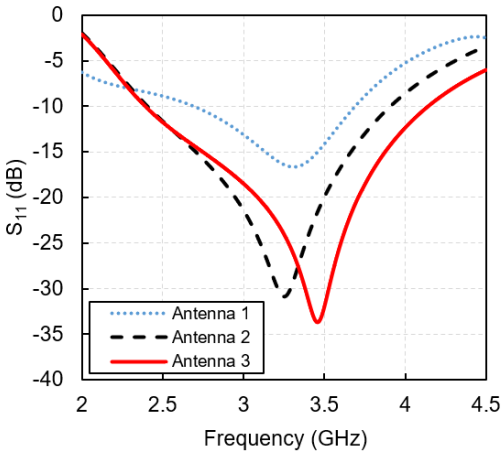

Figure 3. The S_{11} simulation results of the microstrip antenna evolution with several Triple dumbbell-shaped DGS

Antenna 1 has a single dumbbell, Antenna 2 features dual dumbbells, and Antenna 3 incorporates triple dumbbells. Each design represents a step toward enhancing the antenna's bandwidth through the strategic placement of the dumbbell-shaped DGS.

Figure 4 presents the parameter results for S_{11} and FBW for each antenna design. Antenna 1 has a single triple dumbbell-shaped DGS with an S_{11} of -16.65 dB and an FBW of 31.35% (2.69 – 3.69 GHz). Antenna 2 has dual dumbbells. Meanwhile, Antenna 2 shows impedance bandwidth improvement performance, achieving an S_{11} of -30.87 dB and an FBW of 47.47% (2.41 – 3.91 GHz). The last step is Antenna 3, which incorporates triple dumbbells. Antenna 3 has the lowest S_{11} of -33.68 dB and the highest FBW of 53.60% (2.39 – 4.14 GHz). This data suggests that increasing the number of dumbbells results in better antenna performance, particularly in terms of fractional bandwidth.

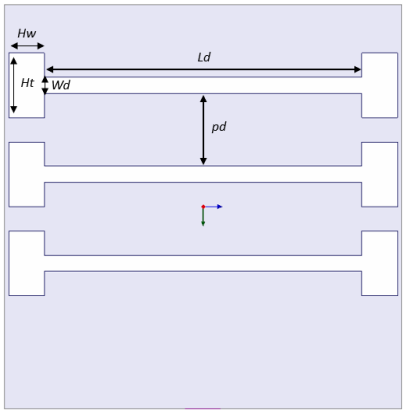

Figure 4. Parameter dumbbell

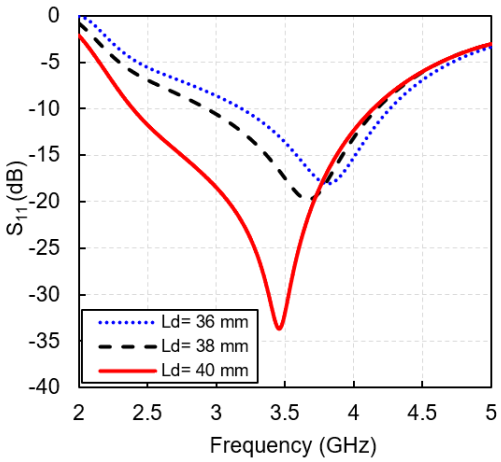

Figure 5. S_{11} simulation results of the dumbbell length, *Ld* parameter

Antenna Design Optimization

Parametric study of the DGS optimization is influenced by some parameters, as shown in Figure 5. The parameters, including *Hw* = 4.5 mm, *Ht* = 8 mm, *Wd* = 2 mm, *Ld* = 40 mm, and *pd* = 9 mm. This stage involves antenna design optimization to achieve optimal bandwidth results. Figure 5 illustrates the parameters of the dumbbell that will be optimized. We have to achieve the best configuration for the impedance bandwidth improvement.

Figure 6 shows the effect of resizing the *Ld* parameter. It presents the relationship between the S_{11} parameter with the dumbbell length (*Ld*). The dumbbell lengths are varied with *Ld* = 36 mm, *Ld* = 38 mm, and *Ld* = 40 mm. In this experiment, only the *Ld* parameter is altered, while all other parameters remain fixed. This allows for the observation of how changes in the dumbbell length influence the antenna's performance, particularly its S_{11} and frequency response.

Table 1 shows that increasing the length of the dumbbell from 36 mm to 40 mm results in a significant improvement in antenna performance, specifically in terms of the minimum S_{11} value. The configuration with *Ld* = 36 mm yields a minimum S_{11} value of -18.02 dB, while *Ld* = 38 mm achieves -30.87 dB, and *Ld* = 40 mm gives the lowest minimum S_{11} value of -33.68 dB. This data indicates that increasing the length of the dumbbell leads to a more significant reduction in the S_{11} value, reflecting an improvement in the antenna's reflection performance at the desired frequency.

In addition, in terms of FBW, it can be observed that increasing the dumbbell length also positively impacts the effective bandwidth. The *Ld* = 36 mm configuration results in an FBW of 29.03%, while *Ld* = 38 mm achieves an FBW of 34.93%, and *Ld* = 40 mm shows the largest FBW of 53.60%. This indicates that a larger dumbbell length not only improves the S_{11} performance but also expands the operational bandwidth, enhancing the overall antenna efficiency.

Figure 7 shows the relationship between the S_{11} parameter and frequency for three variations of the dumbbell height *Ht* (in mm), namely *Ht* = 6.5 mm, *Ht* = 8 mm, and *Ht* = 9.5 mm. In this case, the *Ht* parameter is altered while all other parameters remain unchanged. This allows for the observation of how changes in the thickness of the dumbbell affect the antenna's performance, specifically its S_{11} value and frequency response.

Table 1. Simulation result of dumbbell length, *Ld* parameter

PARAMETER	S_{11}	BW (GHz)	FBW (%)
Ld = 36 mm	-18.02 dB	3.18 – 4.26	29.03
Ld = 38 mm	-30.87 dB	2.93 – 4.17	34.93
Ld = 40 mm	-33.68 dB	2.39 – 4.14	53.60

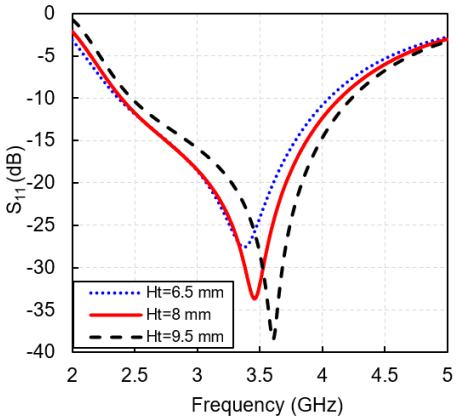

Figure 6. S_{11} simulation results of the dumbbell height, *Ht* parameter

Table 2 summarizes the minimum S_{11} and FBW values for each variation in the dumbbell height, *Ht* parameter. In terms of FBW, the values remain relatively stable within a high range across all *Ht* variations. At *Ht* = 6.5 mm, the FBW was recorded at 52.54%, at *Ht* = 8 mm, the FBW slightly increased to 53.60%, and at *Ht* = 9.5 mm, the FBW decreased to 52.34%. This data suggests that changes in the *Ht* height do not significantly impact the effective bandwidth, indicating a stable performance across different height configurations.

Figure 8 shows that increasing the dumbbell width (*Hw*) from 3.5 mm to 4.5 mm results in a significant decrease in the S_{11} value. At *Hw* = 3.5 mm, the minimum S_{11} value achieved is -20.74 dB, while at *Hw* = 4 mm, the minimum S_{11} value drops to -28.29 dB, and at *Hw* = 4.5 mm, the minimum S_{11} value reaches -33.68 dB. This indicates that increasing the dumbbell width (*Hw*) improves the antenna's performance by lowering the S_{11} value, reflecting better reflection efficiency at the given frequency.

Table 3 summarizes the minimum S_{11} values and the FBW obtained for simulation results of dumbbell width (*Hw*). In addition, it can be observed that increasing the *Hw* also positively impacts the effective bandwidth. At *Hw* = 3.5 mm, the FBW is recorded at 37.18%, while at *Hw* = 4 mm, the FBW increases to 49.48%, and at *Hw* = 4.5 mm, it reaches 53.60%.

Table 2. Simulation result of dumbbell height, *Ht* parameter

PARAMETER	S_{11}	BW (GHz)	FBW (%)
Hw = 3.5 mm	-20.74 dB	2.89 – 4.21	37.18
Hw = 4 mm	-28.29 dB	2.54 – 4.21	49.48
Hw = 4.5 mm	-33.68 dB	2.39 – 4.14	53.60

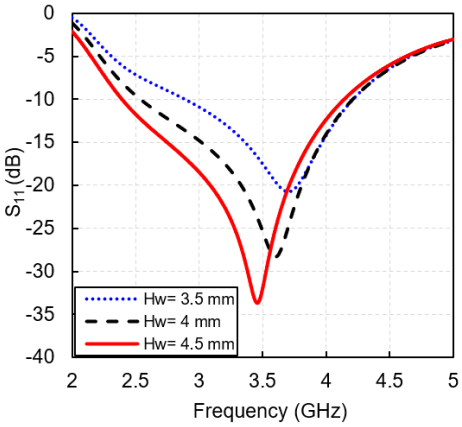

Figure 7. S_{11} simulation results of the dumbbell width, *Hw* parameter

This indicates that a larger *Hw* width not only improves the S_{11} performance but also broadens the operational bandwidth, making the antenna more efficient across a wider frequency range.

Figure 9 shows the relationship between the S_{11} parameter and frequency for three variations of dumbbell bar thickness (*Wd*) that are varied with *Wd* = 1 mm, *Wd* = 2 mm, and *Wd* = 3 mm. In this case, the *Wd* parameter is altered while all other parameters remain fixed. This allows for the analysis of how changing the *Wd* affects the antenna's performance, specifically its S_{11} value and frequency response.

Figure 9 shows the simulation results of the dumbbell bar thickness, *Wd*. The dumbbell bar thickness is varied from 1 mm to 3 mm, and it results in a reduction in the S_{11} value. When *Wd* = 1 mm, the minimum S_{11} value is -14.86 dB, whereas at *Wd* = 2 mm, the minimum S_{11} value decreases to -33.68 dB, and at *Wd* = 3 mm, it reaches -23.15 dB. This indicates that the most optimal performance is achieved at *Wd* = 2 mm, where the lowest S_{11} value is observed, reflecting improved reflection efficiency at the desired frequency.

Table 3. Simulation result of dumbbell width, *Hw* parameter

PARAMETER	S_{11}	BW (GHz)	FBW (%)
Ht = 6.5 mm	-27.57 dB	2.37 – 4.05	52.54
Ht = 8 mm	-33.68 dB	2.39 – 4.14	53.60
Ht = 9.5 mm	-38.49 dB	2.39 – 4.14	52.34

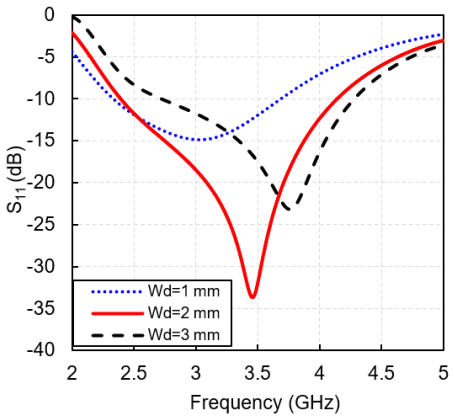

Figure 8. S_{11} simulation results of the dumbbell width, *Wd* parameter

Table 4 Simulation result of dumbbell bar thickness, *Wd*

PARAMETER	S_{11}	BW (GHz)	FBW (%)
Wd = 1 mm	-14.86 dB	2.33 – 3.69	45.18
Wd = 2 mm	-33.68 dB	2.39 – 4.14	53.60
Wd = 3 mm	-23.15 dB	2.72 – 4.28	44.57

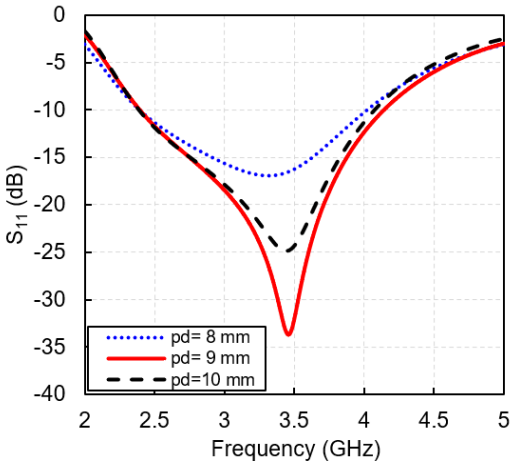

Figure 9. S_{11} simulation results of the dumbbell distance, *pd* parameter

The minimum S_{11} and FBW values for simulation results of dumbbell bar thickness (*Wd*) are summarized in Table 4. In terms of the effective bandwidth FBW, it is evident that the Wd width plays a crucial role. At *Wd* = 1 mm, the FBW was recorded at 45.18%, while at *Wd* = 2 mm, the FBW increased to 53.60%. However, at Wd = 3 mm, the FBW decreased to 44.57%, showing that a larger dumbbell bar thickness (*Wd*) does not necessarily. It leads to better results. This suggests that while increasing Wd can enhance FBW up to a certain point, beyond that, the performance may degrade.

Figure 10 shows the relationship between the S_{11} parameter and frequency for three variations of the *pd* variables. It starts from *pd* = 8 mm, *pd* = 9 mm, and *pd* = 10 mm. The dumbbell spacing, *pd* variables are varied from 8 mm to 9 mm, which leads to a significant improvement in impedance bandwidth performance, particularly in reducing the S_{11} value. At *pd* = 8 mm, the minimum S_{11} value is recorded at -16.90 dB. However, when the two dumbbell spacing (*pd*) increased to 9 mm, the minimum S_{11} value drops considerably to -33.68 dB, indicating a substantial improvement in impedance matching. On the other hand, when the *pd* spacing is further increased to 10 mm, the minimum S_{11} value rises slightly to -24.90 dB, suggesting that the optimal pd spacing for the lowest S_{11} value occurs at *pd* = 9 mm, reflecting the best reflection efficiency at the given frequency.

Table 5. Simulation result of the two dumbbells spacing, *pd*.

PARAMETER	S_{11}	BW (GHz)	FBW%
pd = 8 mm	-16.90 dB	2.39 – 4.02	50.86
pd = 9 mm	-33.68 dB	2.39 – 4.14	53.60
pd = 10 mm	-24.90 dB	2.39 – 4.07	52.01

Table 6. Parameter results without DGS and with DGS

PARAMETER	S_{11}	BW (GHz)	FBW (%)
Without DGS	-20.84 dB	3.47 – 3.53	1.71
With DGS	-33.68 dB	2.39 – 4.14	53.60

Table 5 summarizes the minimum S_{11} values and FBW for each variation of the pd spacing. In terms of FBW, all *pd* variable variations exhibit strong performance, with FBW values exceeding 50%. At *pd* = 8 mm, the FBW is recorded at 50.86%, while at pd = 9 mm, the FBW increases to 53.60%. At *pd* = 10 mm, the FBW slightly decreases to 52.01%. This indicates that the variation in *pd* spacing influences the effective bandwidth, with *pd* = 9 mm yielding the optimal performance.

Table 6 summarizes the S_{11} and FBW results for both the antenna with and without DGS. The antenna without DGS has an FBW of 1.71%, while the antenna with DGS shows a significant improvement, with an FBW of 53.60%. This indicates that the incorporation of DGS not only enhances the impedance matching but also significantly broadens the antenna's bandwidth, making it more efficient and capable of capturing a wider range of frequencies. The antenna with DGS, when configured with parameters *Ld* = 40 mm, *Wd* = 2 mm, *Ht* = 8 mm, *Hw* = 4.5 mm, *Hs* = 3 mm, and *pd* = 9 mm, demonstrates these notable improvements.

RESULTS AND DISCUSSION

Figure 11 presents the results of the fabricated antenna, which measures 50 mm by 50 mm. The fabrication results closely align with the simulation results, demonstrating the accuracy and reliability of the design process. This close match indicates that the fabrication was successful and the antenna performs as expected.Figure 12 compares the simulation and measurement results for the S_{11} parameter across various frequencies. The red line represents the measurement results, while the dashed blue line represents the simulation results. The comparison demonstrates a good agreement between the simulated and measured S_{11} values, indicating that the antenna performs as expected and that the simulation accurately predicts the antenna's real-world behavior.

Table 7 summarizes the comparison of the minimum S_{11} value and FBW between the simulation and measurement results. The simulation results show an FBW of 53.60%, which is slightly higher than the measurement results, which show an FBW of 51.43%.

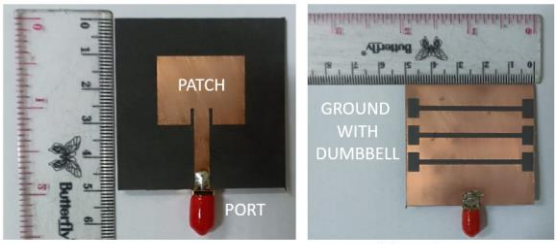

(a) Front View (b) Back View

Figure 11. The Antenna 3 Fabrication

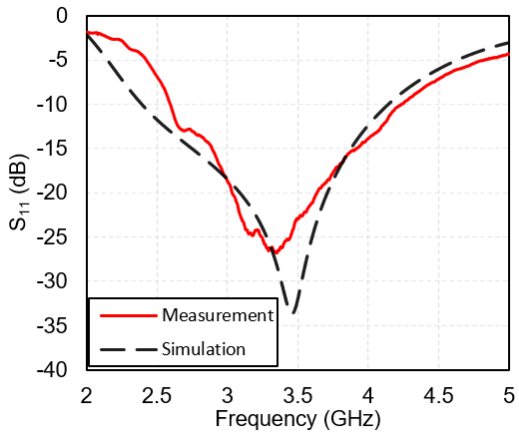

Figure 12. Graph S_{11} Comparison of Simulation and Measurement

Table 7. Parameter Results Simulation and Measurement

PARAMETER	S_{11}	BW (GHz)	FBW%
Simulation	-33.68 dB	2.39 – 4.14	53.60
Measurement	-27 dB	2.6 – 4.4	51.43

This indicates that the simulation tends to predict a slightly broader effective bandwidth compared to the actual measurement results, suggesting a minor discrepancy between the simulated and real-world performance.

Overall, despite the differences between the simulated and measured results, both show a consistent trend in the performance of the S_{11} parameter. The simulated results slightly outperform the measured results, showing a lower minimum reflection value and a wider bandwidth. These differences can be attributed to various factors, such as manufacturing tolerances, environmental conditions during measurement, or other factors not fully accounted for in the simulation, which may cause slight deviations between the predicted and actual antenna performance.

As shown in Figure 13, some differences between the simulated and measured radiation patterns can be observed, with a maximum variation of about 4 dB in certain angular regions. These discrepancies are mainly attributed to practical factors such as fabrication tolerances in the etching process of the Rogers RO5880 substrate, as well as soldering of the SMA connector, which may slightly affect the current distribution on the antenna. In addition, the measurement environment is subject to minor reflections and alignment errors that can alter the measured radiation pattern. Nevertheless, the overall shape of the radiation patterns and the direction of the main lobe remain consistent between simulation and measurement, confirming the validity of the proposed antenna design.

The main lobe direction aligns closely in both patterns, demonstrating good agreement in the antenna's primary radiation characteristics. However, there are noticeable deviations in the side lobes and minor variations in other regions, which suggest potential discrepancies caused by practical factors such as environmental influences, fabrication tolerances, or limitations in the measurement setup.

The measured pattern exhibits more irregularities compared to the smooth simulated curve. These irregularities are likely due to noise or interference during measurement. Despite these differences, the general agreement between simulation and measurement confirms the reliability of the antenna design and its ability to meet the intended specifications.

Figure 14 illustrates the electric field (E-field) distribution around a particular structure at six different phases: 0°, 90°, 180°, and 360°. The colors in the figure represent the intensity of the electric field, with red indicating high field intensity and blue indicating low intensity.

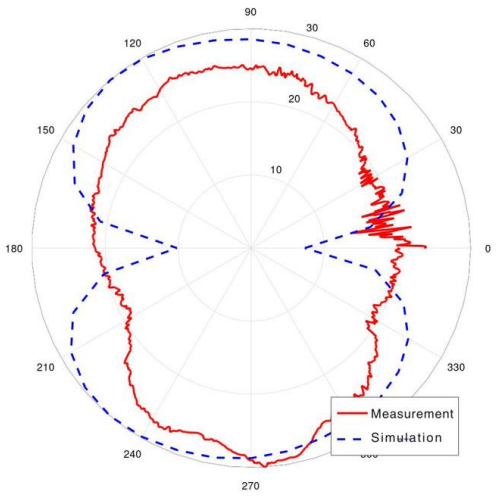

Figure 13. Comparison of simulated and measured Radiation Patterns

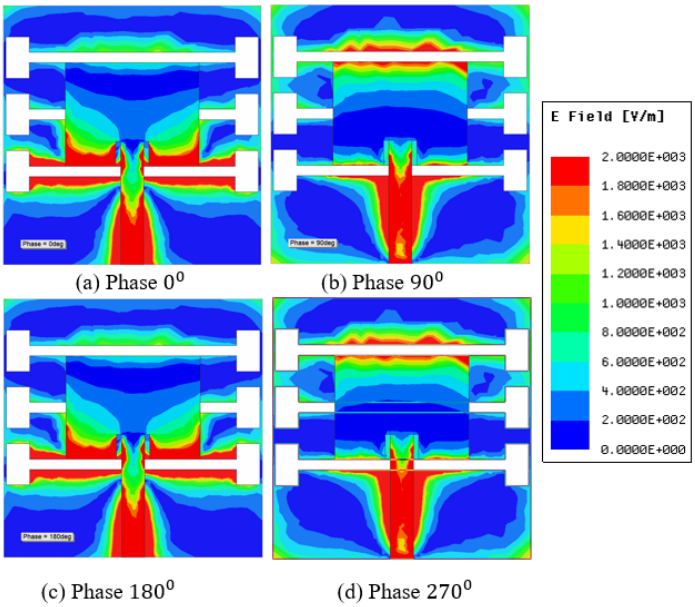

Figure 10 E Field Simulation Results

The electric field distribution at each phase reflects the variation in the resonance pattern, which contributes to the significant enhancement of the antenna's bandwidth performance. This highlights the importance of phase configuration and electric field distribution in designing antennas with improved bandwidth capabilities.

The E-field distribution at phases 0° and 270° appears similar because these two phases are complementary within a full sinusoidal cycle. The electromagnetic wave's oscillation at these points results in a mirrored distribution of the field. This similarity occurs because the sine wave's amplitude at 270° is a reflection of its amplitude at 0°, causing similar E-field patterns. At phases 90° and 180°, the E-field distribution differs due to the wave's oscillatory nature. At 90°, the electric field reaches its maximum positive amplitude, while at 180°, the field transitions to the opposite polarity (negative amplitude). This phase difference alters the way energy is distributed across the structure, resulting in variations in the field pattern. The regions with red coloration, indicating a high E-field intensity, are consistently located at the feeding point and the lower DGS area across all phases.

This phenomenon occurs because the feeding point is the location where the input power is delivered to excite the antenna. This area naturally exhibits a high E-field intensity due to the concentration of electromagnetic energy required to drive the antenna. The DGS introduces localized perturbations in the current distribution, enhancing the field intensity at specific regions.

Table 8. Comparison of Journal Results

Ref.	Freq (GHz)	*FBW*%	*h* (mm)	Sub.	Method
[26]	6	48.67	2.54	RT6006	*Split-Ring Resonator (SRR)*
[19]	3.5	11.11	1.6	FR4	
[20]	3.5	10	1.575	RT5880	
[16]	10	30	1,6	FR4	*Slot patch and DGS*
[17]	10	3.98	1.57	RT5880	*DGS and Perforated Patch Configuration*
[7]	2.4 and 5	38 and 13	1.5	FR4	
[8]	30.5 and 52.4	12.72 and 12.28	0.508	RT5880	DGS
[11]	28	10.53	0.787	RT5880	
This work	3.5	53.60	1.575	RT5880	

The lower DGS acts as a resonating element, trapping and concentrating the electromagnetic energy. This effect is consistent across all phases because the DGS is designed to improve the antenna's performance by enhancing its radiation characteristics and impedance matching.

In addition to the bandwidth performance, the gain, radiation pattern, and radiation efficiency of the proposed antenna were also evaluated to provide a comprehensive

assessment. The simulated gain is 5.13 dBi across the operating band (3.5 GHz), which is consistent with the expected performance of microstrip antennas and indicates that the wide bandwidth is not achieved at the expense of gain. The radiation patterns at representative frequencies of 3.0 GHz, 3.5 GHz, and 4.0 GHz demonstrate a stable broadside main lobe with minor variations in the side lobes, which can be attributed to the wide operating band and fabrication tolerances. Furthermore, the simulated radiation efficiency remains above 80% throughout the band, confirming that the inclusion of the triple dumbbell-shaped DGS does not introduce excessive loss, thereby ensuring efficient performance. In addition, the proposed design maintains a compact size of 50 × 50 mm² using the low-loss Rogers RO5880 substrate, which makes it easy to fabricate and adaptable to other frequency bands by scaling the DGS dimensions. These results demonstrate that the proposed antenna achieves ultra-broadband operation while maintaining high efficiency and design flexibility.

Table 8 provides a comparison of antenna designs utilizing DGS across several studies. A recent study by the researcher, using the Rogers RT5880 substrate with DGS, achieved an FBW of 53.60% (2.39 – 4.14 GHz), which is higher than previous studies, where FBW ranged from 10.53% to 48.67%. As indicated in Table 8, both the current study and previous research have explored antenna designs across various frequency ranges, all incorporating DGS to enhance antenna performance. However, there are notable differences in terms of fractional bandwidth, substrate thickness, and design methodologies, emphasizing the adaptability of antenna design and the impact of specific design parameters on the overall antenna characteristics. This confirms that the proposed triple dumbbell-shaped DGS achieves superior bandwidth performance compared to conventional DGS-based designs, thereby validating the novelty of this work.

Conclusion

This paper has presented an improved microstrip antenna design employing a triple dumbbell-shaped defected ground structure (DGS). Unlike conventional DGS techniques, the proposed configuration introduces a stronger ground-plane perturbation, resulting in superior impedance matching and significant bandwidth enhancement. The antenna achieves a fractional bandwidth of 53.6% in simulation and 51.4% in measurement. Specifically, the ultra-wideband response spans from 2.39 GHz to 4.14 GHz, thereby meeting the criterion of an ultra-broadband antenna.

In addition to its wide bandwidth, the proposed antenna maintains good overall performance, with a simulated gain of 5.13 dBi at 3.5 GHz, stable radiation patterns, and simulated radiation efficiency above 80%. Compared to conventional DGS-based designs that typically achieve only 20–40% FBW, the proposed triple dumbbell-shaped structure demonstrates clear superiority and validates the novelty of this work. Moreover, the compact geometry (50 × 50 mm²) and the use of a low-loss Rogers RO5880 substrate make the design easy to fabricate and adaptable to other frequency bands, thereby confirming both its efficiency and flexibility. These results confirm that the proposed design provides an effective solution for ultra-broadband microstrip antennas and shows strong potential for application in modern wireless communication systems.

REFERENCES

[1] A. Irfansyah, B. B. Harianto, and N. Pambudiyatno, “Design of Rectangular Microstrip Antenna 1x2 Array for 5G Communication,” *Journal of Physics: Conference Series (JPCS)*, vol. 2117, no. 1, 2021, doi: 10.1088/1742-6596/2117/1/012028

[2] S. Abulgasem, F. Tubbal, R. Raad, P. I. Theoharis, S. Lu, and S. Iranmanesh, “Antenna Designs for CubeSats: A Review,” *IEEE Access*, vol. 9, no. March, pp. 45289–45324, 2021, doi: 10.1109/ACCESS.2021.3066632

[3] Y. Zhang and Y. Li, “Wideband Microstrip Antenna in Small Volume Without Using Fundamental Mode,” *Electromagnetic Science*, vol. 1, no. 2, pp. 1–6, 2023, doi: 10.1109/ACCESS.2021.3066632

[4] S. Ermiş and M. Demirci, “Improving the Performance of Patch Antenna by Applying Bandwidth Enhancement Techniques for 5G Applications,” *Tehnički glasnik*, vol. 17, no. 3, pp. 305–312, 2023, doi: 10.31803/tg-20220819001236

[5] J. Zhou, Y. Rao, D. Yang, H. J. Qian, and X. Luo, “Compact Wideband BPF with Wide Stopband Using Substrate Integrated Defected Ground Structure,” *I EEE Microwave and Wireless Components Letters.* vol. 31, no. 4, pp. 353–356, 2021, doi: 10.1109/LMWC.2021.3053756

[6] N. Sakib, S. N. Ibrahim, M. Ibn Ibrahimy, M. S. Islam, and M. M. H. Mahfuz, “Design of Microstrip Patch Antenna on Rubber Substrate with DGS for WBAN Applications,”

2020 IEEE Reg. 10 Symp. TENSYMP 2020, no. June, pp. 1050–1053, 2020, doi: 10.1109/LMWC.2021.3053756

[7] Z. Bendahmane, S. Ferouani, and C. Sayah, "High Permittivity Substrate and DGS Technique for Dual-Band Star-Shape Slotted Microstrip Patch Antenna Miniaturization," *Progress In Electromagnetics Research (PIER) C* vol. 102, no. January, pp. 163–174, 2020, doi: 10.1109/LMWC.2021.3053756

[8] H. M. Emara, S. K. El Dyasti, H. H. M. Ghouz, and M. F. A. Sree, "Design of a Compact Dual-Frequency Microstrip Antenna using DGS Structure for Millimeter-Wave Applications," *Journal of Advanced Research in Applied Sciences and Engineering Technology*, vol. 28, no. 3, pp. 221–234, 2022, doi: 10.37934/araset.28.3.221234

[9] P. A. M. Mercy and M. Arts, "Bandwidth Enhancement of Pentagonal & Circular Microstrip Patch Antenna with DGS for Radar & Satellite Applications," *PriMera Scientific Engineering (PSEN)*, no. April, 2023, doi: 10.56831/PSEN-02-046

[10] D. Rusdiyanto, C. Apriono, D. W. Astuti, and M. Muslim, "Bandwidth and Gain Enhancement of Microstrip Antenna Using Defected Ground Structure and Horizontal Patch Gap," *Sinergi*, vol. 25, no. 2, p. 153, 2021, doi: 10.22441/sinergi.2021.2.006

[11] E. Sandi, B. Maruddani, D. F. Ronald, and R. Ramadhan, "A Wideband Microstrip Triangle Patch Antenna with Double Dumbbell Shaped Defective Ground Structure for 5G Application," *IOP Conference Series: Materials Science and Engineering*, vol. 1098, no. 4, p. 042093, 2021, doi: 10.1088/1757-899X/1098/4/042093

[12] L. Su, J. Munoz-Enano, P. Velez, J. Martel, F. Medina, and F. Martin, "On the Modeling of Microstrip Lines Loaded with Dumbbell Defect-Ground-Structure (DB-DGS) and Folded DB-DGS Resonators," *IEEE Access*, vol. 9, pp. 150878–150888, 2021, doi: 10.1109/ACCESS.2021.3125775

[13] H. M. Emara, S. K. El Dyasti, H. H. M. Ghouz, M. F. A. Sree, and S. Y. A. Fatah, "Compact High Gain Microstrip Array Antenna Using DGS Structure for 5G Applications," *Progress In Electromagnetics Research (PIER) C*, vol. 130, no. March, pp. 213–225, 2023, doi: 10.2528/PIERC22122110

[14] T. Suneetha, S. Alapati, and S. Nagakishore Bhavanam, "Bandwidth Enhancement of Micro Strip Square Patch Antenna with Partial Ground Plane for Wide Band Applications," *International Journal on Engineering Applications (IREA)*, vol. 10, no. 4, pp. 265–271, 2022, doi: 10.15866/irea.v10i4.20442

[15] D. W. Astuti, R. Fadilah, Muslim, D. Rusdiyanto, S. Alam, and Y. Wahyu, "Bandwidth Enhancement of Bow-tie Microstrip Patch Antenna Using Defected Ground Structure for 5G," *Journal of Communication*, vol. 17, no. 12, pp. 995–1002, 2022, doi: 10.12720/jcm.17.12.995-1002

[16] V. Suryanarayana, M. Satya Anuradha, and S. P. Douglas, "Bandwidth Enhancement of Multiwalled Carbon Nanotube Antenna Using Structural Modifications and DGS in X-Band Applications," *Proc. - IEEE 2021 Int. Conf. Comput. Commun. Intell. Syst. ICCCIS 2021*, pp. 792–797, 2021, doi: 10.1109/ICCCIS51004.2021.9397223

[17] A. Gupta and B. Jharia, "Performance Enhancement of 10GHz Patch Antenna using DGS and Perforated Patch Configuration for Advanced Wireless Communication Systems," *SVU-International Journal of Engineering Sciences and Applications*, vol. 5, no. 1, pp. 33–38, 2024, doi: 10.21608/svusrc.2023.229826.1146

[18] D. W. Astuti *et al.*, "Bandwidth Enhancement for Half Mode Substrate Integrated Waveguide Antenna using Defected Ground Structures," *International Journal of Electronics and Telecommunications*, vol. 69, no. 3, pp. 449–454, 2023, doi: 10.24425/ijet.2023.144382

[19] H. H. Ryanu *et al.*, "A Bandwidth and Gain Enhanced Hexagonal Patch Antenna using Hexagonal Shape SRR," *Jurnal INFOTEL*, vol. 16, no. 2, pp. 457–473, 2024, doi: 10.20895/infotel.v16i2.1118

[20] Y. G. Adhiyoga, S. F. Rahman, C. Apriono, and E. T. Rahardjo, "Miniaturized 5G Antenna With Enhanced Gain by Using Stacked Structure of Split-Ring Resonator Array and Magneto-Dielectric Composite Material," *IEEE Access*, vol. 10, pp. 35876–35887, 2022, doi: 10.1109/ACCESS.2022.3163285

[21] N. S. M. Suhaimi, N. M. Mahyuddin, W. Ismail, and I. M. Ibrahim, "Miniaturized 4 × 4 Switched-Beam Butler Matrix with Bandwidth Enhancement for 5G Communication System," *Alexandria Engineering Journal*, vol. 61, no. 12, pp. 13089–13103, 2022, doi: 10.1016/j.aej.2022

.07.014
[22] A. Karimbu Vallappil, M. K. A. Rahim, B. A. Khawaja, and M. N. Iqbal, "Compact Metamaterial Based 4 × 4 Butler Matrix with Improved Bandwidth for 5G Applications," *IEEE Access*, vol. 8, pp. 13573–13583, 2020, doi: 10.1109/ACCESS.2020.2966125
[23] H. H. Tran and N. Nguyen-Trong, "Performance Enhancement of MIMO Patch Antenna Using Parasitic Elements," *IEEE Access*, vol. 9, pp. 30011–30016, 2021, doi: 10.1109/ACCESS.2021.3058340.
[24] V. G. Ajay, T. Mathew, N. V. Krishna Prasad, and M. S. S. R. K. N. Sarma, "Truncated Microstrip Patch Antenna with DGS Based on Double Looped CSRR Arrays for Enhancement of Bandwidth," *Indonesian Journal of Electical Engineering and Informatics (IJEEI)*, vol. 8, no. 3, pp. 593–601, 2020, doi: 10.52549/ijeei.v8i3. 2222
[25] M. K. Adityo, M. I. Nashiruddin, and M. A. Nugraha, "5G Fixed Wireless Access Network for Urban Residential Market: A Case of Indonesia," *Proc. 2021 IEEE Int. Conf. Internet Things Intell. Syst. IoTaIS 2021*, no. September, pp. 123–128, 2021, doi: 10.1109/IoTaIS53735.2021.9628442
[26] V. Rajeshkumar and R. Rajkumar, "SRR Loaded Compact Tri-Band MIMO Antenna for WLAN/WIMAX Applications," *Progress In Electromagnetics Research Letters*, vol. 95, no. October 2020, pp. 43–53, 2020, doi: .org/10.2528/PIERL20100704